JGR Space Physics

RESEARCH ARTICLE
10.1029/2022JA030362

Key Points:

- We observed concurrent occurrence of poleward moving auroral arcs (PMAAs) and Pc5 oscillations on the ground and in the magnetosphere
- We evaluated magnetic energy of Pc5 oscillations and compared it with kinetic energy of precipitating electrons along the field line
- The magnetic energy of Pc5 oscillations is important for auroral emission and simulated the spatial and temporal structures of PMAAs

Correspondence to:
T. Sakurai,
tohrusakurai@mb.scn-net.ne.jp

Citation:
Sakurai, T., Wright, A. N., Takahashi, K., Elsden, T., Ebihara, Y., Sato, N., et al. (2022). Poleward moving auroral arcs and Pc5 oscillations. *Journal of Geophysical Research: Space Physics*, *127*, e2022JA030362. https://doi.org/10.1029/2022JA030362

Received 12 FEB 2022
Accepted 14 JUN 2022

Author Contributions:
Conceptualization: T. Sakurai
Data curation: T. Sakurai, K. Takahashi, T. Elsden, A. Kadokura, Y. Tanaka
Formal analysis: T. Sakurai, K. Takahashi, T. Elsden, Y. Ebihara, N. Sato, A. Kadokura, Y. Tanaka, T. Hori
Funding acquisition: A. N. Wright, K. Takahashi, T. Elsden, Y. Ebihara, N. Sato, Y. Tanaka
Investigation: T. Sakurai, K. Takahashi, Y. Ebihara, N. Sato, A. Kadokura, Y. Tanaka, T. Hori
Methodology: T. Sakurai, K. Takahashi, T. Elsden, Y. Ebihara, N. Sato, A. Kadokura, Y. Tanaka, T. Hori
Resources: T. Elsden
Software: A. N. Wright, T. Elsden, T. Hori
Supervision: A. N. Wright, K. Takahashi, A. Kadokura
Visualization: T. Sakurai, A. N. Wright, K. Takahashi, T. Hori
Writing – original draft: T. Sakurai
Writing – review & editing: A. N. Wright, K. Takahashi, T. Elsden, Y. Ebihara, N. Sato, A. Kadokura, Y. Tanaka, T. Hori

Poleward Moving Auroral Arcs and Pc5 Oscillations

T. Sakurai[1], A. N. Wright[2], K. Takahashi[3], T. Elsden[4], Y. Ebihara[5], N. Sato[6], A. Kadokura[6,7,8], Y. Tanaka[6,7,8], and T. Hori[9]

[1]Tokai University, Hiratsuka, Japan, [2]Mathematical Institute, University of St. Andrews, St. Andrews, UK, [3]The John Hopkins University Applied Physics Laboratory, Laurel, MD, USA, [4]School of Mathematics and Statistics, University of Glasgow, Glasgow, UK, [5]Research Institute for Sustainable Humanosphere, Kyoto University, Uji, Japan, [6]National Institute of Polar Research, Tokyo, Japan, [7]The Graduate University for Advanced Studies, Kanagawa, Japan, [8]Polar Environment Data Science Center, Joint Support-Center for Data Science Research, Research Organization of Information and Systems, Tokyo, Japan, [9]Institute for Space-Earth Environmental Research, Nagoya University, Nagoya, Japan

Abstract We present an example of one-to-one correspondence between poleward moving auroral arcs (PMAAs) and Pc5 oscillations observed at the Time History of Events and Macroscale Interactions during Substorms (THEMIS) Ground Based Observatory station Gillam. The PMAAs consisted of four successive intensifications (named PMAA1, PMAA2, PMAA3 and PMAA4) with a period of 3∼4 min over the magnetic latitudes from 68° to 70° in the auroral oval and varied coherently with the H-component of magnetic field Pc5 oscillations. PMAA1 and PMAA2 appeared clearly at the magnetic latitude ∼69°, and the following two PMAAs, which were dimmer, appeared at the magnetic latitude ∼68°. PMAA1 and PMAA2 exhibited features of field-line resonances with the maximum luminosity at the magnetic latitude ∼69.5° and ∼69.4°, respectively. The ground Pc5 oscillations were concurrent with toroidal mode Pc5 oscillation observed at the THEMIS-D, -E, and -A satellites at ∼4 MLT in the outer magnetosphere. The magnetic and electric field oscillations at THEMIS were synchronized with the PMAAs. The magnetic energy of the THEMIS Pc5 oscillations is estimated using a numerical model of damped toroidal oscillations and compared with the kinetic energy of precipitating electrons associated with the field aligned current carried by the toroidal oscillations. The result reveals that the Pc5 magnetic energy is much larger than the kinetic energy, implying the magnetic energy is important for producing auroral emissions in the ionosphere. We also perform a simulation of the relationship between PMAAs and toroidal mode Pc5 oscillations. The simulation explains the observed spatial and temporal structures of the PMAAs.

Plain Language Summary Aurora are a fascinating phenomenon observed in the polar region of the earth. The auroral emission is caused by the excitation of neutral oxygen atoms and nitrogen molecules in the ionosphere through collision with precipitating electrons from higher altitudes traveling along the magnetic field lines. The precipitating electrons need to have energies of order keV in order to produce auroral emissions. The energy is higher than that of solar wind electrons even after they are heated on passing through the bow shock in front of the magnetosphere. However, how the electrons gain the required high energy is not fully understood. The present study discusses a possible mechanism for the electron acceleration through analysis of the relationship between periodic auroral brightening detected by an all-sky imager and ultralow frequency hydromagnetic (Alfvén) waves detected by the THEMIS spacecraft and a ground magnetometer. The emphasis is placed on the importance of the magnetic energy of Alfvén waves. We find that the magnetic energy is larger than the kinetic energy of the precipitating electrons, implying that the magnetic energy is important for acceleration of auroral electrons. A simulation of this process explains the spatial and temporal structure of the observed auroral emissions.

1. Introduction

The relation between periodic oscillations of auroral arcs and field-line resonances (FLRs) in the Pc5 band has been well known. Samson et al. (1991, 1996) and Xu et al. (1993) presented evidence that the auroral luminosity is modulated with the frequency (1–4 mHz) of simultaneously observed magnetic Pc5 oscillations. They compared the auroral images taken in white light and magnetometer data obtained at the Canadian auroral network for the OPEN Unified Study (CANOPUS) array in Canada and concluded that the precipitation of energetic electrons (energies >3 keV) is modulated with the frequency of Pc5 oscillations. They suggested that the electron precipitation is caused by the kinetic or inertial Alfvén waves (Goertz & Boswell, 1979; Hasegawa, 1976) and/

or electrostatic ion cyclotron turbulence (Hudson et al., 1978; Kindel & Kennel, 1971) and that these kinetic processes are modulated by magnetohydrodynamic (MHD) waves. The relationship between shear Alfvén waves, auroral electron acceleration, and field line resonances have been discussed by Rankin et al. (2005, 2021). They showed that long-period standing waves correlate with redline auroral arcs in the Earth's magnetosphere. They also stressed the importance of a kinetic theory of FLRs since electron bounce motion in long-wavelength standing waves affects the ac conductivity and hence the strength of parallel electric fields. Zhao et al. (2019) presented the first observational evidence from the multi-spacecraft THEMIS mission and a conjugate all-sky imager to support the scenario that standing hydromagnetic waves can generate the quasi-periodic appearance of poleward-moving auroral arcs.

The mechanisms related to high frequency and short scale wavelength electron and ion turbulences have been discussed by Lotko et al. (1998), Chaston et al. (2002), Chaston, Bonnell, et al. (2003), Wygant et al. (2000, 2002), and Keiling et al. (2002) using data from the Polar and Fast Auroral SnapshoT Explorer (FAST) satellites, and by Vaivads et al. (2003) using Cluster and the Defense Meteorological Satellite Program (DMSP) satellite conjunction observations made during auroral activity. Using FAST satellite data Lotko et al. (1998) have noted that in the region of discrete auroral arcs, electrostatic shock and suprathermal electrons were observed when the FLR signatures predicted by MHD theory were observed with optical, magnetic, and radar observations on the ground. Chaston et al. (2002), Chaston, Bonnell, et al. (2003), using FAST satellite observations in the inverted V-region at the altitude of about 4,000 km, have reported that the energy flux density carried by precipitating electrons is similar to the Poynting flux carried by high frequency Alfvén waves. Wygant et al. (2000, 2002) and Keiling et al. (2002), using Polar satellite observations for a short interval, found intense oscillations of the electric and magnetic fields at L = 4–6 in the nightside magnetosphere. At the spacecraft, the Poynting flux associated with the oscillations had a magnitude of 1–2 erg cm^{-2} s^{-1} and was directed toward the ionosphere. When mapped to the 100 km altitude, the magnitude was ∼100 erg cm^{-2} s^{-1}, which is sufficient to power the acceleration of auroral electrons. The downward Poynting flux at Cluster altitudes is comparable to the electron energy flux at low altitudes observed by DMSP (Vaivads et al., 2003).

In this paper we discuss an alternative mechanism for acceleration of electrons based on new observations of PMAAs. We consider the role of large scale FLR Pc5 oscillations in the acceleration of auroral electrons. We evaluate the magnetic energy (W_{FLR}) of Pc5 FLRs using a numerical model of damped toroidal waves on dipole field lines that was used by Takahashi et al. (2019). Note that we use the terms “FLRs” and “toroidal waves” interchangeably, using the latter mainly in describing the wave mode structure along the background magnetic field. The basic equation and algorithm of the numerical model are similar to those used by Newton et al. (1978) and Allan and Knox (1979a, 1979b). To determine whether the FLR have enough energy to drive the electron precipitation, we compare its magnetic energy with the kinetic energy (W_e) of precipitating auroral electrons associated with the FAC carried by the Pc5 FLRs.

The remainder of this paper is as follows: Section 2 describes the data used in this study. Section 3 presents the analysis of the PMAAs and their relation to magnetospheric standing Alfvén waves. Section 4 evaluates the kinetic energy of precipitating electrons driven by the Alfvén waves. Section 5 describes a numerical simulation of PMAAs. A summary and discussion are given in Section 6 and conclusions are given in Section 7.

2. Experiment and Data

Ground-based data used in the present study are auroral all sky images (ASIs) and magnetic field data from the Gillam station (geographic latitude = 56.4°N, geographic longitude = 265.3°E), which is included in the THEMIS Ground Based Observatory (GBO). We also use magnetic and electric field vector observations from the THEMIS-D, -E, and -A satellites, which were located in the outer magnetosphere (Angelopoulos, 2008; Mende et al., 2008). The original ASIs had 752 × 580 pixels, but the resolution is reduced to 256 × 256 pixels by averaging, corresponding to a spatial resolution of ∼1 km at zenith at 110 km altitude (Donovan et al., 2006). We use the altitude-adjusted corrected geomagnetic (AACGM) coordinate system (Shepherd, 2014) to specify locations at the ionospheric height 110 km and use the symbols λ_{AACGM} and φ_{AACGM} for the latitude and the longitude in this system. Gillam is located at λ_{AACGM} = 65.8°N and φ_{AACGM} = 333.7°E. In addition, we use ground magnetometer data from the Churchill Chain stations of the University of Alberta. The Churchill Chain station

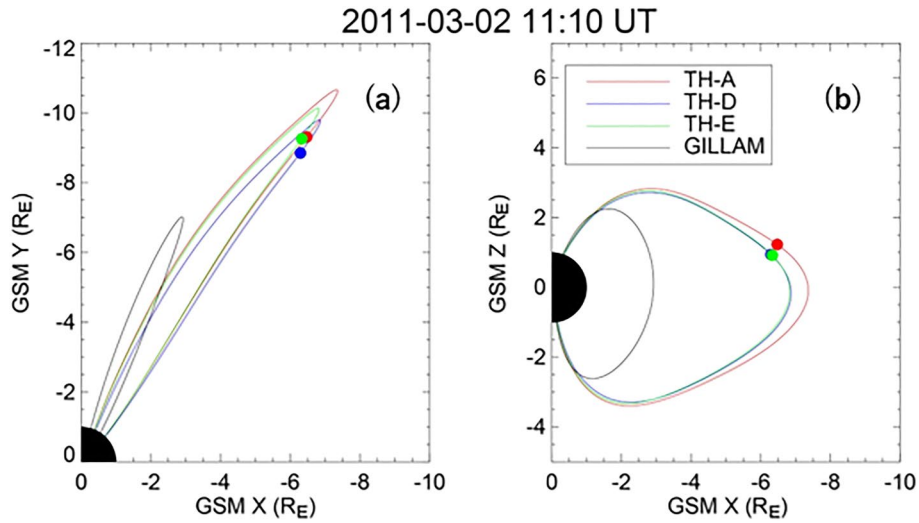

Figure 1. TS05 model magnetic field lines passing through Gillam (black), THEMIS-D (blue), - E (green), and -A (red) at 11:10 UT on 02 March 2011. The solid circles indicate the satellites. (a) Projection to the geocentric solar magnetospheric (GSM) *X-Y* plane. (b) Projection to the geocentric solar magnetospheric (GSM) *X-Z* plane.

magnetometer data are available through the CARISMA data at the University of Alberta (http://www.carisma.ca/station-information).

Figure 1 shows the magnetic field lines passing through the THEMIS-D, -E, and -A satellites and the ground station Gillam at 11:10 UT on 02 March 2011. The field lines are given by the TS-05 model (Tsyganenko & Sitnov, 2005) and projected to the *X-Y* (Figure 1a) and *X-Z* planes (Figure 1b) of geocentric solar magnetospheric (GSM) coordinates. During the selected period PMAAs and Pc5 oscillations were observed simultaneously at Gillam and the THEMIS- satellites. The satellites traversed the dawn-side outer magnetosphere near the magnetic equatorial plane at Z_{GSM} ~1.5 RE (Figure 1b).

Figure 2 shows the footprints of the satellites at 110 km altitude mapped on the Gillam ASI image at 11:12 UT during the appearance of PMAAs. The tick marks are plotted at every 30 min from 10:30 to 11:30 UT. The satellite footprints pass the recurring optical horizontal structures of PMAAs. The satellites traversed in the field of view of the ASI from the east (right) to the west (left). During this interval the auroral arcs were extended horizontally in the east-west direction and moved poleward periodically (the north is upward in the image) with a period of ~4 min.

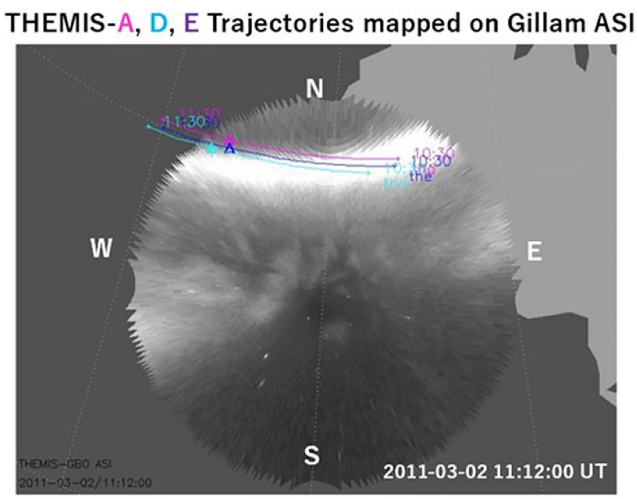

Figure 2. Trajectories of THEMIS- A, -D, and -E from 10:30 to 11:30 UT mapped on the all sky image (ASI) obtained at Gillam at a selected epoch, 11:12:00 UT on 02 March 2011. The center of the ASI is the zenith, the north and south directions are the top and bottom of the image, and the west and east are the left and right, respectively. The crosses and triangles indicate the satellite positions at 30 min intervals.

3. Data Analysis

3.1. Poleward Moving Auroral Arcs (PMAAs) and Magnetic Field Pc5 Oscillations

Figure 3 illustrates the temporal and spatial variations of the PMAAs and their relation to the ground Pc5 pulsations. Figure 3a is a keogram that is generated from the ASI time series with the vertical axis being λ_{AACGM}. PMAA1 and PMAA2 were observed clearly at the higher magnetic latitudes λ_{AACGM} ~ 69°. PMAA3 and PMAA4, which are weaker, appeared at lower latitudes λ_{AACGM} ~ 68°. Figure 3b shows the luminosity oscillation at λ_{AACGM} = 68.76°, and Figure 3c shows the H-component Pc5 magnetic field oscillations at TALO, FCHU, GILL and ISLL. The optical and magnetic oscillations have nearly identical periods, and a ~180° phase shift is recognized between the luminosity oscillations and Pc5 oscillations observed at GILL. The Pc5 amplitude at FCHU is the largest among the stations and the phase at this station is delayed by ~90° with respect to GILL. The phase at

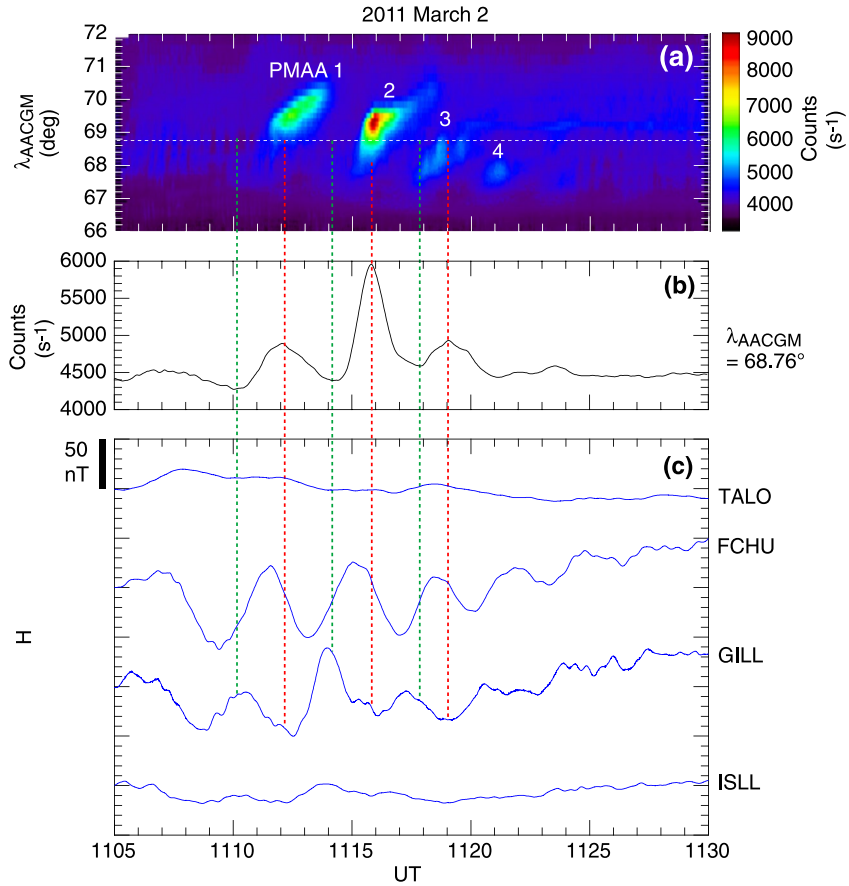

Figure 3. (a) Keogram generated from the all sky image (ASI) slices along the magnetic meridian at Gillam. Numbers are assigned to prominent peaks. The vertical axis shows the AACGM latitude (λ_{AACGM}). (b) Luminosity variations at $\lambda_{AACGM} = 68.76°$ (horizontal dashed line in panel (a)). The vertical lines indicate the minima (green) and maxima (red) of the luminosity. (c) Magnetic field H-component at the Churchill Chain stations, TALO ($\lambda_{AACGM} = 78.14°$, $\varphi_{AACGM} = 332.18°$), FCHU (68.19°, 334.27°), GILL (66.03°, 333.36°) and ISLL (63.52°, 334.02°).

ISLL leads a little with respect to GILL. The poleward shift of the phase and the amplitude maximum at FCHU indicate that field line resonance occurred with its center close to FCHU.

The H-component Pc5 oscillations are attributed to the ionospheric Hall current driven by the horizontal electric field of standing Alfvén waves. The waves carry FACs, which are associated with the bright and dark portions of the PMAAs. These signatures suggest that the generation of the PMAAs is related to FACs associated with the Pc5 oscillations.

3.2. Luminosity Oscillations Versus Magnetic Latitude

Figure 4 shows the temporal variations of the luminosity (photon counts) at five magnetic latitudes. The identified luminosity peaks are numbered. The peaks at higher latitudes are time delayed from those at the lower latitudes. By inspecting Figure 3a we find that the strongest luminosity peak occurred at $\lambda_{AACGM} = 69.4°$ for PMAA2, and the second strongest peak occurred at $\lambda_{AACGM} = 69.5°$ for PMAA1. The latitudinal difference between these two peaks is only about 0.1°, corresponding to about 10 km at the 110 km height in the ionosphere. Evidently, all sky keogram analysis (Humberset et al., 2017) provides a much higher spatial resolution than that obtained using ground magnetometers.

At the lower latitudes (Figures 4c–4e), the luminosity oscillations are different. Peaks occur more regularly with similar intensities. The oscillation periods (~180 s) are shorter than at the higher latitudes (~240 s), and there is little phase delay among the three lower latitudes. This absence of the phase delay on a latitude dependence

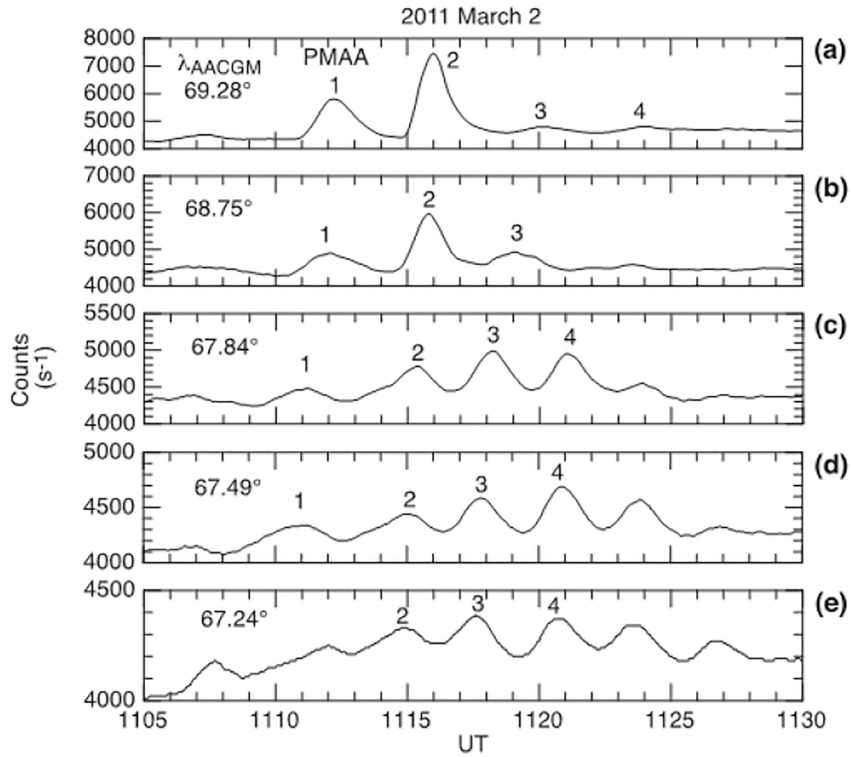

Figure 4. Temporal variations of luminosity at five latitudes, from (a) $\lambda_{AACGM} = 69.28°$ to (e) $\lambda_{AACGM} = 67.24°$. The luminosity peaks are numbered.

suggests that the field lines connected to the aurora are on the same side of the resonant field line (Wright & Allan, 1996).

Figure 5 shows the λ_{AACGM} dependence of the peak amplitude of the luminosity oscillations normalized at $\lambda_{AACGM} = 66.45°$. The main features in this figure are: (a) the amplitude initially increases at the higher latitudes (PMAA1 to PMAA2); (b) then it decreases (PMAA3 to PMAA4); (c) the latitudinal width of the peaks initially narrows (PMAA1 to PMAA2); and (d) then broadens. These features can all be understood in terms of the behavior of standing Alfvén waves that are driven by a fast mode wave for a couple of cycles in the presence of dissipation through Joule heating and electron acceleration (Wright & Allan, 1996).

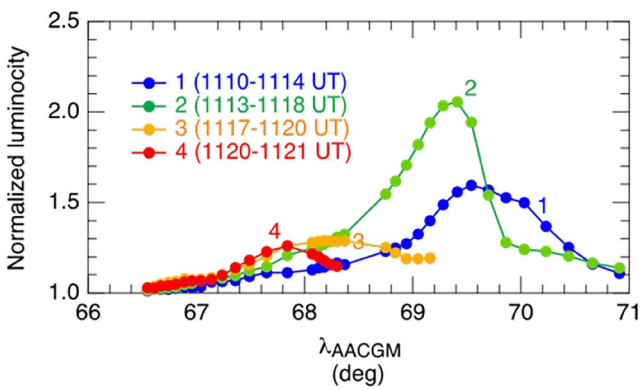

Figure 5. Latitudinal variations of auroral luminosity (relative intensity) for PMAA1 (blue), PMAA2 (green), PMAA3 (orange), and PMAA4 (red). The luminosity is normalized to the value at $\lambda_{AACGM} = 66.45°$.

Field lines have natural Alfvén frequencies ω_A, which depend on latitude (λ). Figure 3a of Wright (1992) shows the FLR amplitude response of the Alfvén waves in terms of $\omega_A(\lambda)$ for a finite duration monochromatic driving signal that could represent the fast mode driving the FLR. After having been driven for only one cycle, the maximum amplitude of the Alfvén wave is actually on field lines for which $\omega_A < \omega$, where ω is the frequency of the fast mode. As the Alfvén waves are driven for more cycles the maximum Alfvén wave amplitude moves toward the field line for which $\omega_A = \omega$, so will move to lower latitudes as seen in Figures 4 and 5.

While driven by the fast mode, the Alfvén fields grow secularly in time, which accounts for the increase in amplitude between PMAA1 and PMAA2. This is enhanced further when it is noted that the arc luminosity depends on the FAC which depends on the amplitude of the Alfvén wave magnetic field divided by the latitudinal scale, which initially will vary as the phase-mixing length, $L_{ph} = 2\pi/(td\omega_A/d\lambda)$ (Mann et al., 1995).

The fact that PMAA2 has the largest amplitude suggests the fast mode driving the Alfvén waves only lasted a couple of cycles. Subsequently, the Alfvén

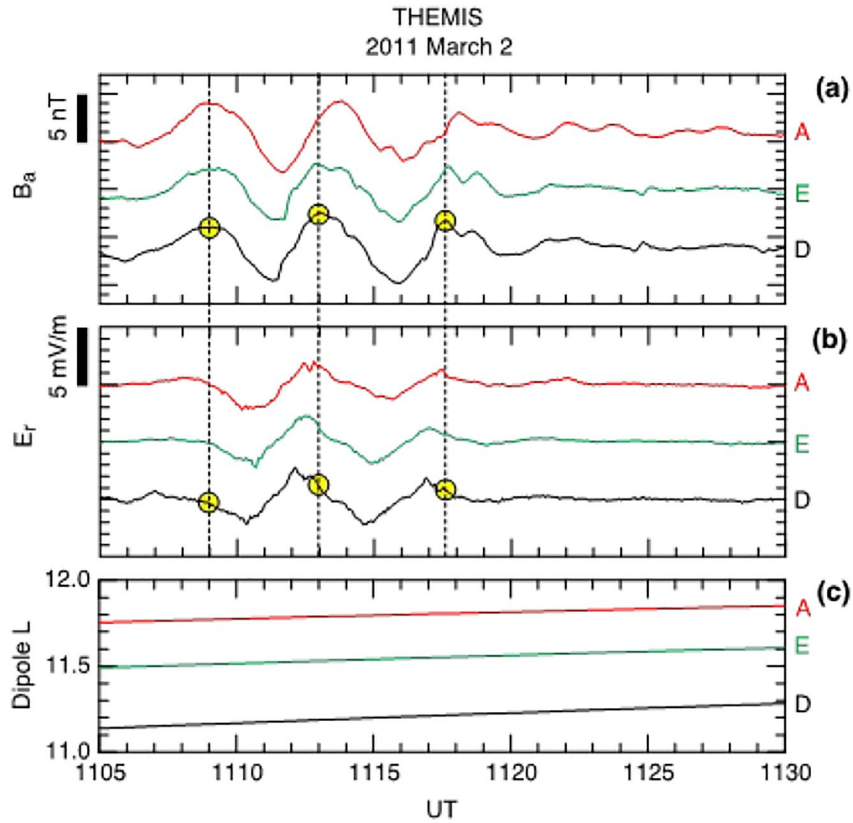

Figure 6. Pc5 waves observed by THEMIS-A (red), -E (green), and -D (black). (a) Azimuthal component of the magnetic field. Vertical dashed lines are drawn through the prominent peaks at THEMIS-D (yellow filled circles). (b) Radial component of the electric field. The crossing points of the vertical dashed lines are marked by yellow filled circles for THEMIS-D. (c) Dipole *L* values of the spacecraft.

waves decay in amplitude as they lose energy through ionospheric heating and electron energization, and this accounts for the decrease in amplitude in time of PMAA3 and PMAA4.

3.3. Comparison Between PMAAs at Gillam and Pc5 Oscillations at THEMIS

Figure 6 shows the intense Pc5 oscillations of the azimuthal component of the magnetic field (B_a) and the radial component of the electric field (E_r) observed by THEMIS-A, -E, and -D from 11:05 to 11:30 UT. These field components are shown using the mean field aligned (MFA) coordinate system described by Takahashi and Denton. (2021). The MFA coordinate axes are defined using a reference magnetic field ($\mathbf{B}_{ref}$) and the spacecraft position vector **R** relative to the center of the Earth. The reference field $\mathbf{B}_{ref}$ is obtained by fitting a function to the three components of the observed B-field vector time series given in geocentric solar ecliptic (GSE) coordinates. The function is a polynomial of the form $c_0 + c_1\tau + c_2\tau^2 + c_3\tau^3 + c_4\tau^4$, where τ is UT rescaled to the range from −0.5 to 0.5 for the data segment selected for analysis. The coefficients c_0–c_4 are determined using the least squares method. In the MFA coordinate system, the parallel or compressional (p) component is in the direction of $\mathbf{B}_{ref}$, the azimuthal (a) component (positive eastward) is in the direction of $\mathbf{B}_{ref} \times \mathbf{R}$, and the radial ($r$) component is given by $\mathbf{e}_r = \mathbf{e}_a \times \mathbf{e}_p$. The transverse components Br and Ba are perturbations about $\mathbf{B}_{ref}$ by definition, and the compressional perturbation is given by $B_p - |\mathbf{B}_{ref}|$.

Intense oscillations are clearly seen from 11:10 to 11:20 UT. This interval corresponds to the PMAAs and Pc5 oscillations observed at Gillam examined earlier. The amplitudes at the spacecraft are 2–4 nT (B_a) and 2–3 mV/m (E_r). The period is longer at THEMIS-A, which had the highest L. Also note that B_a has a ∼90° phase delay from E_r (compare yellow filled circles), as expected for standing Alfvén waves (Takahashi et al., 2019).

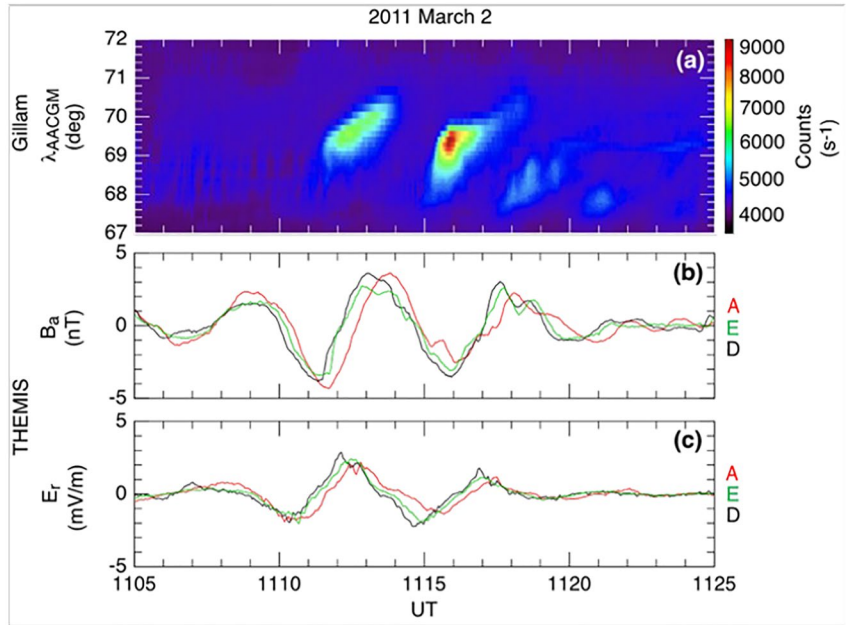

Figure 7. (a) Keogram of the poleward moving auroral arcs (PMAAs). (b) Magnetic field azimuthal components at THEMIS-D (black), -E (green), and -A (red). (c) Same as (b) but for the radial components of the electric field.

The standing Alfven waves are most likely excited as the fundamental mode from a model calculation of the mode frequency. In this calculation, we solved the Singer et al. (1981) standing wave equation for the TS05 magnetic field line passing through the THEMIS-E location at 11:15 UT. We adopted a $1/r$ mass density variation along the field line, where r is the geocentric distance. The model fundamental frequency matches the observation (4 mHz) if we assume an equatorial mass density of 0.3 amu/cc. Although no mass density data is available from THEMIS, the mass density value appears to be reasonable.

Figure 7a shows the PMAAs observed at Gillam and the B_a (Figure 7b) and E_r (Figure 7c) components of the Pc5 oscillations at THEMIS. The time intervals of PMAAs and the Pc5 wave packet agree well and suggest that these are related. However, the oscillation periods at the satellites are a little longer than those of the PMAAs. This may be due to the difference of the magnetic field lines passing through the optical aurora and the satellites as already shown in Figure 1. THEMIS-D, -E, and -A were located at $L \sim 11.2$, $L \sim 11.5$, and $L \sim 11.7$, respectively, while the PMAAs appeared at the magnetic latitude, 69°–71°, which corresponds to $L = 8.5$–10.4 in the dipole field.

The concurrent occurrence of the PMAAs and Pc5 oscillations suggests that they are produced by a common driver external to the magnetosphere. Changes in the solar wind dynamic pressure (Claudepierre et al., 2010; Kepko et al., 2002) and disturbances in the foreshock (Wang et al., 2019) are known drivers of magnetospheric Pc5 waves. To find possible solar wind sources of the Pc5 waves, we generated Figure 8 using the 1 min solar wind OMNI data (time shifted to the bow shock nose) and the magnetic field data from Cluster-2 (Balogh et al., 1997), geosynchronous GOES-13 and GOES-15 (Singer et al., 1996), and THEMIS-D. The positions of the satellites are shown in Figure 8a. The bulk velocity (Figure 8b) and the dynamic pressure (Figure 8c) were steady at ~600 km/s and ~2 nPa, respectively, although the data gaps make it difficult to discuss short-period changes. The interplanetary magnetic field (IMF) data are more continuous. The IMF cone angle Θ_{xB} ($= \cos^{-1}(|B_x|/B)$) (Figure 8e) decreased from >80° at 11:00 UT to ~60° after ~11:02 UT.

The IMF B_{zGSM} component (Figure 8d) changed little with the negative value ~−4 nT over the time interval, meaning that the cone angle change is primarily due to a change of the field orientation in the X-Y plane. Such a change can produce a disturbance in the foreshock, which in turn generates transient Pc5 waves in the magnetosphere (e.g., Wang et al., 2019).

The magnetic field magnitude B_T at Cluster-2 (Figure 8f) indicates that the spacecraft moved between the magnetosheath (lower magnitude with irregular variations) and the magnetosphere (higher magnitude). A magnetosheath

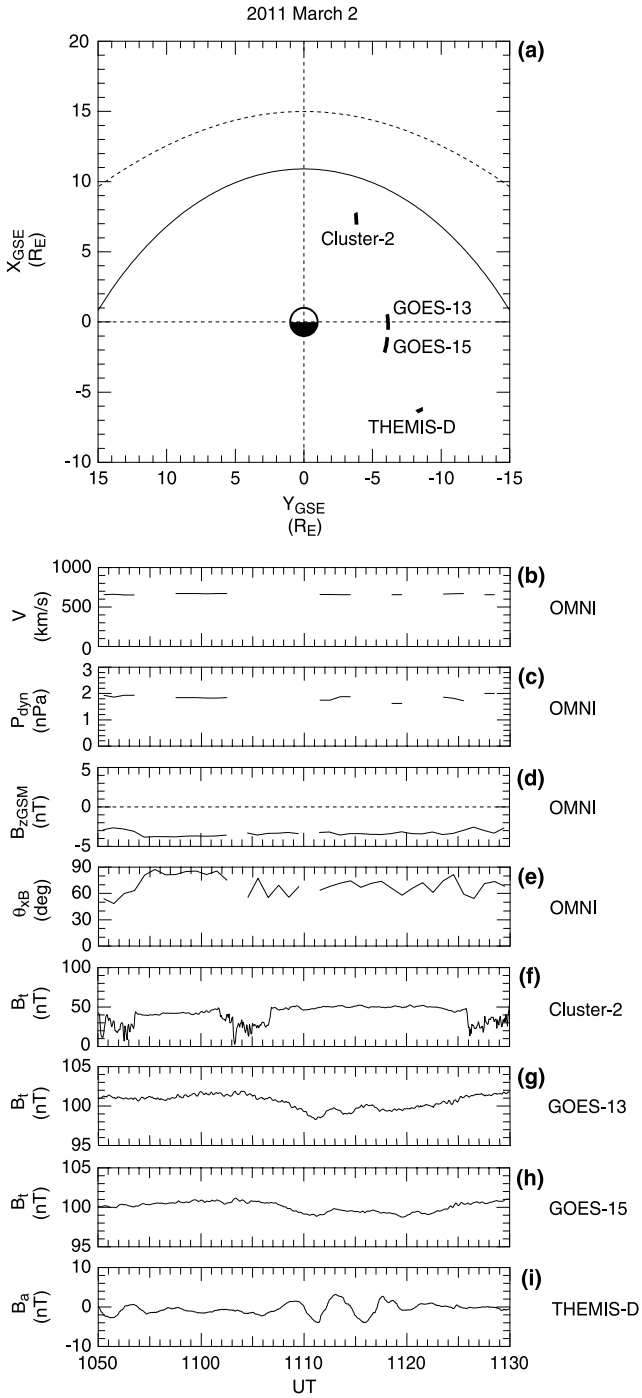

Figure 8. (a) Satellite positions projected to the geocentric solar ecliptic (GSE) equatorial plane. (b, c, d, and e) Solar wind parameters taken from the OMNI-1 min data covering the time interval of the selected Pc5 event. (b) Bulk velocity. (c) Dynamic pressure. (d) Interplanetary magnetic field (IMF) B_z component in geocentric solar magnetospheric (GSM) coordinates. (e) IMF cone angle. (f–h) Magnetic field magnitude at Cluster- 2, GOES-13, and GOES-15. (i) Azimuthal component of the magnetic field at THEMIS-D.

entry means an inward motion of the magnetopause. The magnetoseath entries of Clueter-2 at 10:50–10:53 UT and 11:02–11:07 UT are associated with cone angle changes seen in the OMNI data, suggesting that foreshock disturbances briefly compressed the magnetosphere. The magnetic field magnitude at GOES decreased after 11:07 UT in association with the entry of Cluster-2 into the magnetosphere. The Cluster and GOES observations can be attributed to an expansion of the magnetosphere. We suggest that the toroidal oscillation at THEMIS-D (Figure 8i) was triggered by this magnetospheric expansion.

4. Evaluation of Magnetic and Electron Kinetic Energies

In this section we evaluate magnetic energy associated with the toroidal mode fundamental Pc5 oscillations on the magnetic field line passing through the THEMIS-A satellite ($L = 11.76$).

4.1. Magnetic Energy of Pc5 Oscillations Observed by the THEMIS Satellite

The magnetic energy of Alfvén wave FLR contained in a flux tube of a unit area at the ionosphere is defined as follows:

$$W_{\mathrm{FLR}} = \int \frac{B_a{}^2}{2\mu_0} \mathrm{d}V \tag{1}$$

where B_a is azimuthal component magnetic field of FLR Pc5 oscillations and μ_0 is magnetic permeability of free space. For a dipole field the volume element of the tube dV can be expressed in terms of the magnetic latitude (λ):

$$\mathrm{d}V = A_{\mathrm{I}} \frac{B_{\mathrm{I}}}{B(\lambda)} r_{\mathrm{eq}} \cos\lambda (1 + 3\sin^2\lambda)^{\frac{1}{2}} \mathrm{d}\lambda \tag{2}$$

Here r_{eq} is the equatorial distance of the field line; A_I is the ionospheric cross-section of the flux tube; B_I is the equilibrium field strength at the highest magnetic latitude $\lambda = 73.04°$, $B_I = 59{,}587$ nT. $B(\lambda)$ is the equilibrium magnetic field strength at the magnetic latitude λ.

If we take $A_I = 1$ (unit area), then we can compare the precipitated electron energy that is calculated in Section 4.2. This will allow us to see how much energy has gone into the upward current electrons (W_e) compared to the energy of the FLR flux tube (W_{FLR}). We anticipate that W_e will be a fraction of W_{FLR} and could be used to estimate the damping effect of electron energization on the FLR for this event. If $W_{FLR} < W_e$, then there will not be enough energy in the FLR to energize the electrons.

We now estimate the magnetic energy W_{FLR} using Equation 1: the azimuthal component of magnetic field (B_a) versus magnetic latitude (λ) is given in Figure 9, in which B_a is the value estimated utilizing the damped toroidal FLR dipole model of the fundamental mode Pc5 oscillations used by Takahashi et al. (2019) under the assumption of the ionospheric Pedersen conductivity $\Sigma_P = 7$ mho, which is typical of observed values during the auroral activity in the morning side ionosphere (Robinson et al., 1987). In Figure 9 Ba is normalized to the value B_{aI} at the ionospheric foot point located at $\lambda = 73.04°$.

THEMIS-A was located at a magnetic latitude $\lambda = 10.1°$ where the normalized model B_a (B_{aM}) is 0.013. To match B_a observed at THEMIS-A ($B_{a,ThA}$)

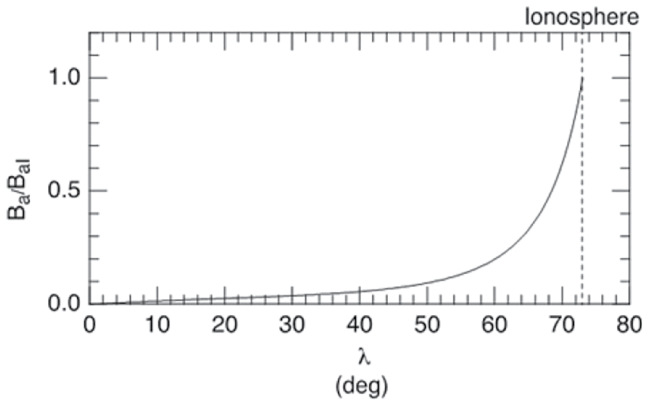

Figure 9. Magnetic latitude dependence of the B_a amplitude of the model toroidal wave at $L = 11.76$, normalized to the value B_{aI} at the ionospheric foot point located at $\lambda = 73.04°$ (vertical dashed line).

we need to scale this value to be 4 nT (so it coincides with the THEMIS-A in-situ observation):

$$B_{a,\mathrm{ThA}} = \frac{B_{\mathrm{aM}} \times 4.0}{0.013} \tag{3}$$

This allows the FLR wave magnetic energy density ${B_{a,\mathrm{ThA}}}^2/2\mu_0$ to be calculated.

Here we define $B_I/B(\lambda)$ taking the highest magnetic latitude to be the ionosphere, where $B_I = 59{,}587$ nT,

$$\frac{B_I}{B(\lambda)} = \frac{59,587 \times 10^{-9}}{B(\lambda)} \tag{4}$$

We then work out the integrand of Equation 1 on a grid of latitudinal steps for a unit cross section at the ionosphere ($A_I = 1$ m^2) to evaluate the integral.

The result is the magnetic energy of the flux tube passing through THEMIS-A that has unit cross section at the ionosphere.

$$W_{\mathrm{FLR}} = 2.27\mathrm{J/m}^2 \tag{5}$$

We compare this with the precipitated electron kinetic energy W_e, which is estimated in the next section.

4.2. Estimation of FAC

Before estimating the precipitating electron kinetic energy we have to evaluate the FAC at the ionosphere associated with Pc5 oscillations observed by the THEMIS-A satellite. Using the in situ observation the azimuthal component ($B_{a,\mathrm{ThA}}$) of the magnetic field Pc5 oscillations, $B_{a,\mathrm{ThA}} = 4$ nT at the magnetic latitude $\sim 10.1°$ we obtain the corresponding value of the magnetic field at the altitude 110 km in the ionosphere, $B_{a,\ 110\ \mathrm{km}} = 301.34$ nT (at the highest latitude $\lambda = 73.04°$), which is estimated by the model calculation using the toroidal dipole damped model of the fundamental mode Pc5 oscillation. With this value we estimate $J_{||}$ value at the ionosphere using the formula presented by Greenwald and Walker (1980):

$$\mu_0 J_{||} = \frac{B_{a,110\,\mathrm{km}}}{\Delta x} \tag{6}$$

$$J_{||} = \frac{B_{a,110\,\mathrm{km}}}{\mu_0 \Delta x} = \frac{301.34 \times 10^{-9}}{\left(4\pi \times 10^{-7}\right)(110 \times 1{,}000)} = 2.2\,\mu\mathrm{A/m}^2 \tag{7}$$

Here Δx is resonance width in the north-south direction at an altitude of 110 km in the ionosphere and can be estimated based on the scale of the PMAA. From the luminosity curve of PMAA2 shown in Figure 5 we calculate $I_{\max}/\sqrt{2}$, where $I_{\max}$ is the luminosity maximum and $I_{\max}/\sqrt{2}$ is an effective luminosity used to determine the latitudinal width (Δx) of the PMAA. $I_{\max}/\sqrt{2}$ is a definition of resonance width of LCR circuit (Agarwal & Lang, 2005). The value of $I_{\max}$ is 8,222 at $\lambda_{\mathrm{Imax}} = 69.41°$ and $I_{\max}/\sqrt{2}$ is 5,755 at $\lambda_1 = 69.70°$, $\lambda_2 = 68.65°$. Hence the difference in the latitude is $1.05° \simeq 1°$, and we adopt 110 km (1° in latitude) for the width (Δx) in the calculation of 7. Resonance width 110 km corresponds to that of the normalized amplitude (0.7) of Pc5 based on the relation of Pc5 wave amplitude versus radial scale length by Glassmeier and Stellmacher (2000) and the resonance width of STARE radar observation of toroidal mode electric field Pc5 pulsations by Greenwald and Walker (1980).

4.3. Estimation of Electron Kinetic Energy (W_e)

The FAC of Alfvén waves is mainly carried by electrons traveling parallel to the magnetic field. During the upward current phase, magnetospheric electrons travel downward to the ionosphere. In large-amplitude Alfvén

waves the current densities reach a few μA/m^2 above the ionosphere and the electrons achieve energies of the order of keV. When the electron motion is dominated by the parallel velocity component, the B/n_e curve is central to interpreting the electron energization: B/n_e has a peak around 0.56 R_E above the ionosphere (Wright & Hood, 2003), below which ionospheric electrons are trapped. The energization of electrons actually occurs at and above the B/n_e peak. We can use the values of $J_{||}$, n_e, and $V_{e||}$ at the B/n_e peak to estimate the electron energy flux there. As there is negligible electron acceleration below the B/n_e peak, electrons will simply follow the converging field lines to the ionosphere and the energy flux will increase according to the flux tube cross section (or field strength). If we use a subscript "p" to denote the value at the B/n_e peak, we first need to find the electron energy flux at the B/n_e peak.

Kinetic energy flux $(K_{E\_flux})_p$ at the B/n_e peak is

$$(K_{E\_flux})_p = \frac{1}{2} m_e n_{e,p} V_{e||,p}^3 \tag{8}$$

and can be scaled to get the flux at the ionosphere, $(K_{E\_flux})_I$

$$(K_{E\_flux})_I = \frac{1}{2} m_e n_{e,p} V_{e||,p}^3 \frac{B_I}{B_p} \tag{9}$$

Multiplying this flux by the duration of upward FAC phase ($\sim T/4$, where T is the Pc5 oscillation period) gives

$$W_e = \frac{1}{2} m_e n_{e,p} V_{e||,p}^3 \frac{B_I}{B_p} \frac{T}{4} \tag{10}$$

The aim is to compare this with the Alfvén wave magnetic energy (W_{FLR}) at the ionosphere, which has been obtained in the previous section. Before this comparison we need to evaluate the electron kinetic energy flux at the B/n_e peak. The FAC at the B/n_e peak can be estimated using the FAC at the ionosphere, $J_{||,I} = 2.2$ μA/m^2.

The magnetic latitude (λ) of the B/n_e peak (λ_p) along the field line passing through $L = 11.76$ is $\lambda_p = 68.07°$ and the equilibrium field strength at the B/n_e peak is $B_p = 1.5599 \times 10^{-5}$ T. We also need the equilibrium field strength at the ionosphere, $B_I = 5.95879 \times 10^{-5}$ T. (The magnetic latitude of the ionosphere is $\lambda_I = 73.04°$).

The ratio of the field strengths, $R_{I/p}$ is:

$$R_{I/p} = \frac{B_I}{B_p} = \frac{5.95789}{1.5599} = 3.82 \tag{11}$$

The FAC at the B/n_e peak is

$$J_{||,p} = \frac{J_{||,I}}{R_{I/p}} = \frac{2.2 \times 10^{-6}}{3.82} = 5.76 \times 10^{-7} \text{A/m}^2. \tag{12}$$

The FAC $J_{||}$ can be related to the electron velocity,

$$J_{||} = -q n_e V_{e||} \tag{13}$$

where $q = 1.60 \times 10^{-19}$ C. The magnetospheric upward current-carrying electron density (n_e) is taken to be 1 cm^{-3}. This gives the electron velocity at the B/n_e peak to be

$$V_{e||,p} = |-\frac{J_{||}}{q n_{e,p}}| = \frac{5.76 \times 10^{-7}}{1.6 \times 10^{-19} \times 10^6} = 3.60 \times 10^6 \text{ m/s}. \tag{14}$$

Hence, the accelerated electron kinetic energy flux at the B/n_e peak, $F_{e,p}$ is

$$F_{e,p} = \frac{1}{2} m_e n_{e,p} V_{e||,p}^3 = 0.5 \times 9.1 \times 10^{-31} \times 10^6 \times \left(3.60 \times 10^6\right)^3 = 2.12 \times 10^{-5} \text{J/m}^2\text{s} \tag{15}$$

And the corresponding ionospheric flux ($F_{e,I}$) is

$$F_{e,I} = F_{e,p} \times R_{I/p} = \left(2.12 \times 10^{-5}\right) \times 3.8 = 8.1 \times 10^{-5} \text{J/m}^2\text{s}. \tag{16}$$

Table 1
Dependence of the Peak Altitude of B/n_e on the n_m/n_0 Ratio for Fixed Scale Height h of 400 km

n_m/n_0	$B/n_{e,p}$ altitude (R_E)
500	0.51
1,000	0.56
2,000	0.60

During the upward FAC phase ($T/4$ = 56.5 s) the electron kinetic energy added to the ionosphere for unit area (A_I = 1 m^2) is:

$$W_e\left(n_{e,p} = 1.0\text{cm}^{-3}\right) = F_{e,I}\frac{T}{4} = \left(8.1\times10^{-5}\right)\times 56.5(\text{s}) = 0.0046\,\text{J/m}^2. \quad (17)$$

If instead we take the magnetospheric upward current-carrying electron density at the B/n_e peak to be $n_{e,p}$ = 0.1 cm^{-3}, that is, 10^5 m^{-3}, then $F_{e,I}$ is 100 times larger than that of when the electron density n_e = 1 cm^{-3}:

$$W_e\left(n_{e,p} = 0.1\text{cm}^{-3}\right) = 0.46\,\text{J/m}^2. \quad (18)$$

This is the kinetic energy density of the precipitating electrons in J/m^2. It can be compared with the Alfvén wave magnetic energy W_{FLR} obtained in the previous section, W_{FLR} = 2.27 J/m^2, such that

$$\frac{W_e}{W_{FLR}} = \frac{0.46}{2.27} = 0.20 \quad (19)$$

The result shows that the precipitating electron kinetic energy is only 20% of the magnetic energy (W_{FLR}). Therefore, W_{FLR} has enough power to produce auroral emissions in the ionosphere. The electron kinetic energy W_e drains energy from the FLR and has the effect of damping the Alfvén waves in the ionosphere. This mechanism acts in addition to Joule dissipation in the ionosphere.

Our results are obviously sensitive to the values we adopt for various key parameters, and it is worth checking how these values affect our conclusions. We assumed the altitude of the B/n_e peak to be 0.56 R_E (Wright & Hood, 2003). Wright and Hood (2003) assumed that the number density of magnetospheric ions (n_0) is constant along the field line whereas the number density of ionospheric ions is stratified by gravity with a scale height (h). The maximum ion density at the base of the F region is denoted by n_m. They obtained 0.56 R_E for the n_m/n_0 ratio of 10^3 and h of 400 km. As shown in Tables 1 and 2, the altitude of the B/n_e peak does not change significantly when we vary the n_m/n_0 ratio from 500 to 2,000, and h from 300 to 500 km, and hence, the result $W_e < W_{FLR}$ is robust.

Combining Equations 12–16, we obtain

$$W_e = \frac{1}{2}m_e\left(\frac{J_{||I}}{q}\right)^3\left(\frac{1}{n_{e,p}R_{I/p}}\right)^2\frac{T}{4} \quad (20)$$

and see W_e is inversely proportional to the square of $n_{e,p}$. We have also assumed that $n_{e,p}$ is 0.1 cm^{-3}. If 0.1 cm^{-3} is close to the lower limit of the electron density in the plasma sheet (Ishisaka et al., 2001), the calculated W_e value will be the upper limit. That is, the ratio W_e/W_{FLR} provided in (19) should be regarded as the upper limit.

5. Simulation of PMAAs

In order to simulate the main features of the observed PMAAs, we utilize the numerical model of Wright and Elsden (2020), the main features of which are described briefly here. The model solves the linear magnetohydrodynamic (MHD) equations under the cold plasma approximation, in a background 3-D dipole magnetic field. The standard orthogonal, field-aligned 3-D dipole coordinates (e.g., Kageyama et al., 2006) are optimized for numerical efficiency (see Section 2 and Figure 1 of Wright & Elsden, 2020). This allows for unprecedented resolution perpendicular to the magnetic field, making the model perfectly suited for studying FLRs, which can develop small perpendicular scales due to Alfvén wave phase-mixing. For example, in the simulations we present, the radial resolution (grid spacing) in the equatorial plane is 1/20 R_E.

Table 2
Dependence of the Peak Altitude of B/n_e on the Scale Height h for Fixed n_m/n_0 Ratio of 10^3

h (km)	$B/n_{e,p}$ altitude (RE)
300	0.43
400	0.56
500	0.68

Another advantage of using such a code is the ability to tailor the plasma equilibrium to the problem at hand. In this case, the plasma density is set to reproduce a realistic monotonic decrease in the toroidal Alfvén frequency outside of the plasmasphere. In particular, the variation of the frequency is chosen to match that in the optical data at latitudes similar to where the PMAAs were observed. The simulation domain extends from the southern

to northern ionosphere, where perfectly reflecting (infinite conductivity) boundary conditions are enforced. The inner boundary in L-shell is placed at $L = 5$ R_E and also has a boundary condition of perfect reflection, to model the sharp density change present at the plasmapause. The outer boundary in the model is set by the Shue magnetopause (Shue et al., 1997), with a chosen subsolar point location of $L = 10$ R_E. Energy flow into the magnetotail is simulated by the addition of a dissipative buffer region, beginning at $X = -7$ R_E, such that waves do not return the solution region of interest (the dayside magnetosphere). Dissipation is provided in the model through resistivity, such that the width of phase-mixed FLRs can be limited and always resolved. Full details on the dissipation profiles are provided in Section 3.4 of Wright and Elsden (2020).

Since the event in question was observed on the dawn flank during high-speed solar wind flow, it is possible that the PMAAs were excited by the Kelvin Helmholtz instability on the flank magnetopause at dawn or even just antisunward propagating transient disturbances associated with the changes in solar wind conditions. As previously mentioned, the outer boundary of the simulation domain used in the model is the magnetopause, so does not include magnetosheath flow. This means a self-consistent model of the production of the disturbance at the magnetopause is not possible. However, the effect of the solar wind on the magnetosphere can be studied by applying a pressure perturbation on the magnetopause boundary that causes it to move in a similar fashion to if there were a magnetosheath flow and KH instability or antisunward propagating transients present. The fact that the PMAAs appear as a packet of four arcs suggests that changes in the solar wind may have temporarily excited the KH instability on the flank, which in turn excited a finite number of PMAAs.

To devise a suitable form of pressure to apply to the magnetopause we restrict driving on the dawn flank from 4.8 to 9.7 MLT where conditions are favorable for exciting the KH instability. The period of the PMAAs (in Figure 3a) should be similar to the frequency of the KH instability, and was taken to be 226 s. This is the value of the period we adopt for the pressure perturbation we apply to the magnetopause. To simulate the gusty nature of the likely driver we do not apply a monochromatic driver to the magnetopause, but a rather finite duration signal that ramps up in amplitude over 1 cycle, remains steady for 2 cycles, then ramps down smoothly to zero over an additional cycle. This choice was motivated by the optical signatures of the PMAAs.

The response of the waves in the magnetosphere is expected to be similar to the observations reported earlier in this paper. To facilitate comparison of observations with the simulation, we use the simulation results to mimic the PMAAs optical signature on the dawn flank. (The simulation used ~6 MLT, but the arcs are extended over several hours of local time.) The results are shown in Figure 10 and have been normalized so the peak upward current matches the 2.2 μA/m^2 obtained in Subsection 4.2. The keogram in Figure 10 is indicative of the likely auroral emissions in a similar format to that in Figures 3a and 7a.

The auroral luminosity is proportional to the precipitating electron energy flux, which is proportional to $J_{\parallel}^3$, with the caveat that the energy flux must be greater than about 1 mW/m^2 or $J_{\parallel}$ greater than about 1 μA/m^2 at the ionosphere (Chaston, Peticolas, et al., 2003). Figure 10 mimics these properties by plotting the cube of the upward current to represent the precipitating electron energy flux above a particular threshold. To generate the keogram we set the threshold current to be 1.4 μA/m^2 which is consistent with a precipitating energy flux of 1 mW/m^2 if the number density of magnetospheric electrons carrying the upward current at the B/n_e peak is 0.14 cm^{-3}. (This assumes the B/n_e peak is at an altitude of 4,334 km.) The peak upward current of 2.2 μA/m^2 has a corresponding precipitating electron energy flux of 4 mW/m^2 which is consistent with values that are expected to generate auroral arcs.

It is interesting to note that the fourth PMAA is centered at a latitude 1.5° lower than the first PMAA in both data of Figure 3a and the simulation in Figure 10. Additional simulations (not shown) confirm that the change in latitude correlates with the Alfvén frequency $\omega_A(\lambda)$ and its variation with latitude. Figure 3a of Wright (1992) shows the FLR amplitude response for a finite duration monochromatic signal that could represent the fast mode driving the FLR. If the signal has a frequency ω, then after many cycles the FLR amplitude is peaked where $\omega_A(\lambda) = \omega$, as expected. However, after just one cycle the largest FLR amplitude peaks on field lines for which $\omega_A(\lambda) < \omega$, and could explain why the first PMAA appears at a higher latitude (lower ω_A) than the fourth PMAA.

Note that the broadband driving supplied by the disturbance on the magnetopause finished at around $t = 14$ min, so the oscillations after this time are essentially free oscillations at the local frequency $\omega_A(\lambda)$. It is evident that the period of luminosity variation at 71° is longer than that at 68° consistent with the $\omega_A(\lambda)$ variation. This frequency variation is associated with a latitudinal phase speed (given by the slope of the features in the keogram). Figure 10a

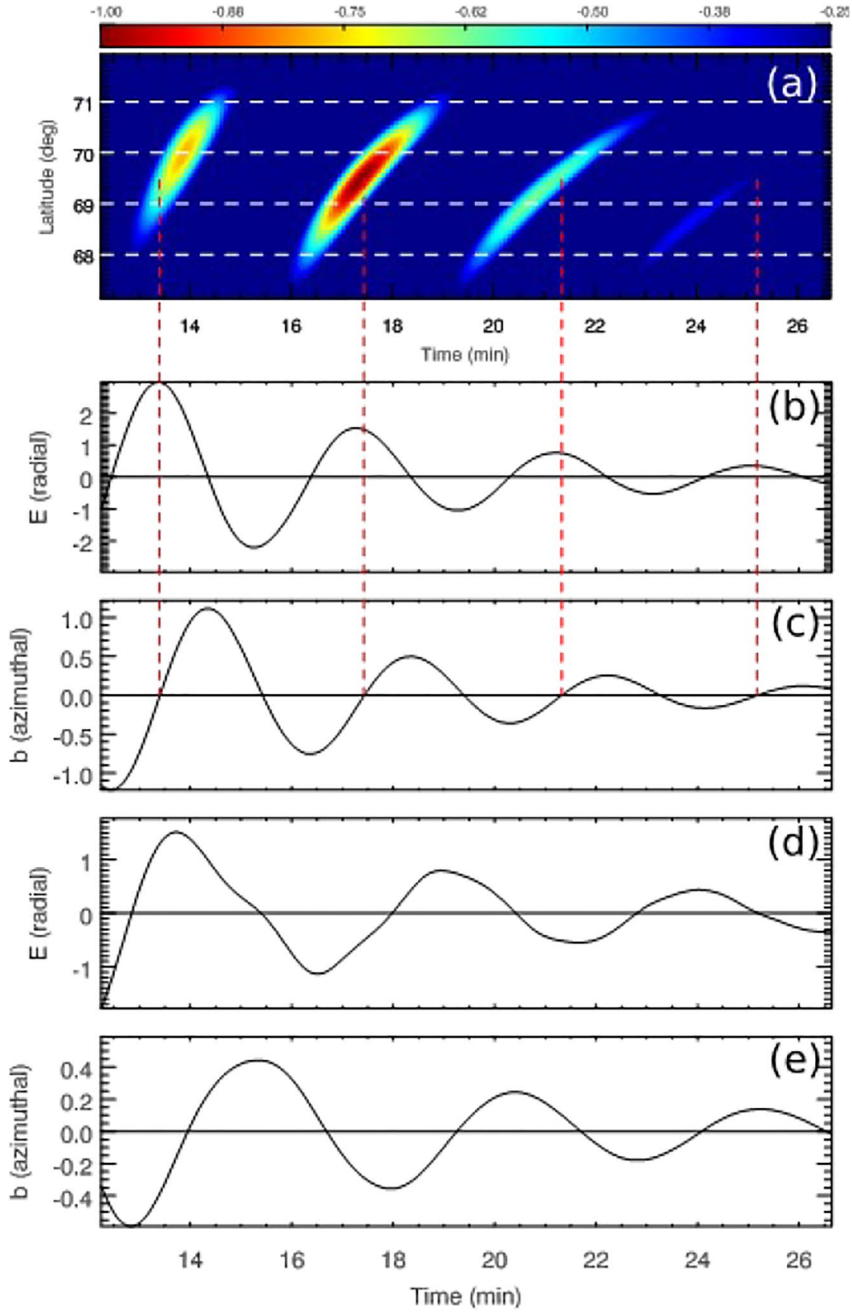

Figure 10. Simulation keogram similar to the data in Figures 3a and 7a on the dawn flank (~6 MLT). Panel (a) shows the down going precipitating electron energy flux, which is proportional to auroral luminosity. The energy flux has been normalized by its maximum magnitude (4 mW/m^2) for which the corresponding upward current is 2.2 μA/m^2. (The color bar is linear and covers the dimensional energy flux range from −1 m to −4 mW/m^2. The negative sign indicating a downward flow of energy.) Panels (b and c) show E and b data from a virtual satellite on the L-shell ($L = 8.18$) mapping a latitude of 69.5°. The red dashed lines show the correlation between nodes of azimuthal magnetic field and peak luminosity at this latitude. Panels (d and e) show E and b data from a virtual satellite at a higher L shell ($L = 10.12$) which maps to a latitude of 71.68°. At this location the wave period is similar to that observed by THEMIS, so panels (a, d, and e) are similar to Figure 7. (E and b are given in normalized simulation units).

is strikingly similar to Figure 7a of Elsden and Wright (2018) who studied the phase motion across L-shells of FLR perturbations produced by a broadband excitation in a 3D magnetosphere. They were able to model the change in phase speed over time using results from Wright et al. (1999) who showed how the key quantity was the gradient of ω_A (see their Equation 4). Converting their formula to a latitudinal phase velocity gives

$$V_{ph} = \frac{-\omega_A(\lambda)}{\left(\frac{d\omega_A}{d\lambda}\right) t}$$

and the $1/t$ dependence accounts for the fact that inclination of the auroral luminosity structures in Figure 10a changes in time. This is consistent with similar phase velocity properties reported by Zhao et al. (2019) from both modeling and observations. Figure 7b of Elsden and Wright (2018) confirms the $1/t$ phase velocity variation and shows how the change in slope can be used to predict the time at which the impulsive broadband driver was applied.

Panels (b and c) of Figure 10 show the radial electric and azimuthal magnetic fields observed by a virtual simulation satellite on the L-shell $L = 8.18$ (which maps to a latitude of 69.5°). The red dashed lines originate at nodes of the azimuthal magnetic field and are when the latitudinal gradient of the magnetic field will be a maximum—that is, the FAC is a maximum. We have only indicated the lines corresponding to a maximum of upward current, and it is evident that these correlate very closely with the maximum auroral luminosity at a latitude of 69.5°, consistent with the expectation that the FLR is responsible for producing the PMAA.

In the real data presented earlier, the THEMIS satellites were not on the same L-shells as the PMAAs, but located at larger L. This is consistent with the fact that the FLR fields observed by THEMIS (Figures 7b and 7c) have a longer period than the PMAAs (Figure 7a). We can reproduce this feature in the simulation by placing a virtual satellite on $L = 10.12$ (latitude 71.68°) and we show the corresponding FLR fields in Figures 10d and 10e. (Note the tight correlation between nodes of magnetic field and auroral emission peaks no longer exists.) The satellite electric and magnetic fields shown in Figures 7 and 10 are in quadrature, with the radial electric field leading the azimuthal magnetic field. This is consistent with the picture of a standing Alfvén wave observed by a satellite in the northern hemisphere and is similar to the THEMIS data shown in Figures 6 and 7.

6. Discussion

We can summarize our study as follows:

6.1. Summary

1. Concurrent occurrence of Poleward Moving Auroral Arcs (PMAAs) and magnetic field Pc5 oscillations is observed.
2. The maximum luminosities of the PMAAs were observed at the magnetic latitudes, $\lambda_{AACGM} = 69.54°$, 69.41°, 68.18°, and 67.8°, for the PMAA1, PMAA2, PMAA3, and PMAA4, respectively, confined within two degrees in the high latitude of the auroral zone.
3. These PMAAs exhibited periodic oscillations with a period of 3–4 min, concurrent with the magnetic field H-component of Pc5 oscillations observed at Gillam ($\lambda_{AACGM} = 66.18°$N).
4. The latitudinal variations of the luminosity indicate that the PMAAs represent FLR oscillations. Their FLR amplitude response is consistent with a theoretical description of driving by a finite duration fast mode wave.
5. The luminosity variations are closely correlated with the H-component magnetic field Pc5 oscillations observed on the ground. The bright and dark parts correspond to the negative and positive excursions of the H-component Pc5 magnetic field oscillations. The implication of this observation is that both periodic oscillations are closely related to FACs, that is, the upward and downward FACs corresponding to the bright and dark parts of the luminosity variations and also to the negative and positive excursions of the H-component magnetic field Pc5 oscillations observed on the ground, respectively.
6. The magnetic energy contained in the Alfvén wave FLR fields (W_{FLR}) is sufficient to account for the energy lost through accelerating electrons (W_e) to carry the FAC.

7. Simulation of the PMAAs compares well with the PMAAs shown in the auroral keogram obtained at Gillam. The simulation is performed with a code designed for simulating FLRs in the Pc5 frequency band by Wright and Elsden (2020).

6.2. Excitation of PMAAs in Relation to FLR Pc5 Oscillations

In this study we found clear evidence for one-to-one correspondence between PMAAs and H- component of Pc5 magnetic field oscillations. The H component Pc 5 oscillations observed on the ground were concurrent with fundamental toroidal mode oscillations observed by THEMIS satellites in the magnetosphere. The luminosity variations of PMAAs exhibited features consistent with FLR Pc 5 oscillations. These observations imply that PMAAs are closely related to FACs associated with toroidal mode oscillations and lead to the periodic reappearance of PMAAs similar to those in the simulation described in Section 5.

The simulation was driven for a couple cycles on the magnetopause flank by a pressure perturbation with a period matching the PMAA period in Figure 3a and was normalized so the peak upward current matches the 2.2 $\mu A/m^2$ obtained in Section 4.2. The keogram in Figure 10 is indicative of the likely auroral emissions in a similar format to that in Figures 3a and 7a. Simulations of time-dependent fast-Alfvén wave coupling give the evolution of the FAC, which can excite PMAAs with properties like those in the observations. Specifically, the variation in intensity of successive PMAA can be matched, as well as their poleward phase motion and drift to lower latitudes.

The FAC $J_{||}$ is estimated as 2.2 ($\mu A/m^2$) at the ionosphere, which corresponds to 4 (mW/m^2) when we assume the upward current-carrying magnetospheric electron density to be 0.14 (cm^{-3}) at the B/n_e peak. These values satisfy the threshold values, 1($\mu A/m^2$) and 1 (mW/m^2) for exciting auroral emission (Chaston, Peticolas, et al., 2003). The value of electron density we adopt (0.14 cm^{-3}) at the B/n_e peak is consistent with observations by the Akebono (Exos D) satellite (Sakanoi et al., 1995) and the Reimei satellite (Fukuda et al., 2014).

In Sections 4.1 and 4.3 we examined the magnetic energy (W_{FLR}) of Pc5 oscillations and compared it with the precipitating electron kinetic energy (W_e) carried by FACs. Comparing these energies reveals that ~20% of W_{FLR} is dissipated through the acceleration of auroral electrons during the upward current interval ($T/4$), suggesting a strong damping of Alfvén waves during a couple of cycles. This result seems to be consistent to the observed PMAAs: the PMAAs exhibited a very short duration, that is, with the amplitude being large initially for PMAA1 and PMAA2, then dimmer for PMAA3 and PMAA4.

We evaluated the magnetic energy of Pc5 oscillations using large scale MHD waves, that is, damped type toroidal mode fundamental oscillations along magnetic field line in this study. Wright et al. (2002, 2003) have noted the importance of nonlinear electron dynamics for electron acceleration by Alfvén waves. This approach should be taken into account in future studies.

The damping of the FLR through losing energy to accelerate precipitating electrons is an additional loss mechanism to that associated with Joule heating of the ionosphere. The FLR model used (Takahashi et al., 2019) included a finite Pedersen conductivity so had a complex natural frequency with $\omega_i/\omega_r = 0.16246$. The damping time is $\sim 1/\omega_i$ and the period is $\sim 2\pi/\omega_r$ so ohmic heating alone will damp the FLR over $\sim \omega_r/(2\pi\omega i) \sim 1$ periods. This suggests that electron energization is a less important sink of energy than ohmic heating. This could be rephrased as stating that the FLR studied can comfortably afford to energize the electrons needed to carry the FACs. The fact that the PMAA persist for several periods (despite an ohmic decay time of 1 period) is consistent with the assumption made in the simulations that the FLRs need to be driven for a couple of cycles. Subsequently, once the FLRs are no longer driven, they decay over 1–2 cycles.

It is interesting to note that if the FLR amplitude is held fixed, but the latitudinal scale is reduced, the ohmic heating will not change, but the energy required to accelerate electrons may increase dramatically (Wright et al., 2003), so in other events electron acceleration may provide a more significant sink of FLR energy.

7. Conclusions

We provided clear evidence for one-to-one correspondence between PMAAs and Pc5 magnetic field oscillations. It suggests that there is a strong correlation between the generation of PMAAs and the upward and downward FACs. The THEMIS satellites observed Pc5 oscillations in the morning side outer magnetosphere, concurrent

with the PMAAs and ground Pc5 oscillations at Gillam. The magnetic energy of Pc5 oscillations and the kinetic energy of precipitating electrons associated with FACs are examined. We found that the electron kinetic energy is only 20% of the magnetic energy, suggesting that magnetic field of Pc5 oscillations has an important role for accelerating precipitating auroral electrons in the ionosphere. In addition, we conducted a numerical simulation of PMAAs and obtained an explanation of the spatial and temporal properties of observed PMAAs.

Data Availability Statement

The CARISMA data are available through the open data repository at U. Alberta. http://www.carisma.ca/station-information. The data used to produce the simulation plots can be accessed at the site. https://figshare.com/authors/Tom_Elsden/4743264. The THEMIS data are available through the open data repository at UC Berkeley. http://themis.ssl.berkeley.edu/index.shtml. The SPDF-Coordinated Data are available through the open data repository at NASA. https://cdaweb.gsfc.nasa.gov. The GOES magnetometer data are available from NOAA. https://satdat.ngdc.noaa.gov/sem/goes/data/full. The Cluster magnetometer data are available from NASA. https://cdaweb.gsfc.nasa.gov.

Acknowledgments
This study was supported by National Institute of Polar Research (NIPR) through General Collaboration Projects, Project Research No. 30-1 in 2019, and Project Research No. 2.2 in 2020–2021, and was performed using computing system of the Communications and Computing Science Center of NIPR. This work was partially supported by a grant-in-Aid for Scientific Research C (15K05305) and the Inter-university Upper atmosphere Global Observation NETwork (IUGONET) project funded by the Ministry of Education, Culture, Sports, Science and Technology of Japan. A.N. Wright's participation was through a program sponsored through the International Space Science Institute, and was partially funded by the Science and Technology Facilities Councils (STFC) grant (ST/N000609/1). K. Takahashi was supported by NASA Grant NNX17AD34G and NSF grant 1744609. T. Elsden was funded by an Early Career Fellowship, split jointly by the Leverhulme Trust (ECF-2019- 155). T. Elsden acknowledges funding by the University of Leicester and the University Glasgow. This study was supported by JSPS KAKENHI grants 20H01960, and Research Institute for Sustainable Humanosphere (RISH), Kyoto University, Mission Research 3 and Flagship Collaborative Research. The authors acknowledge NASA contract NAS5-02099 and V. Angelopoulos for the THEMIS- Mission data, S. Mende and E. Donovan for the ASI data, S. Mende and C. T. Russell for the THEMIS Ground-based Observatories (GBO). We acknowledge Churchill Chain magnetometer at TALO, FCHU, GILL and ISLL. The Churchill Chain magnetometer is Part of the CARISMA network operated by U. Alberta (Ian Mann, PI). The data analysis of the THEMIS Mission was performed through the TDAS, SPEDAS (Angelopoulos et al., 2019), IUGONET (Hayashi et al., 2013) and the NIPR computer facilities. The authors acknowledge J. H. King and N. Papitashvili for use of OMNI data through SPDF-Coordinated Data.

References

Agarwal, A., & Lang, J. (2005). *Foundations of analog & digital electronic circuits*. Elsevier.
Allan, W., & Knox, F. B. (1979a). A dipole model for axisymmetric Alfvén waves with finite ionosphere conductivities. *Planetary and Space Science*, *27*(1), 79–85. https://doi.org/10.1016/0032-0633(79)90149-1
Allan, W., & Knox, F. B. (1979b). The effect of finite ionospheric conductivities on axisymmetric toroidal Alfvén wave resonances. *Planetary and Space Science*, *27*(7), 939–950. https://doi.org/10.1016/0032-0633(79)90024-2
Angelopoulos, V. (2008). The THEMIS mission. *Space Science Reviews*, *141*(1–4), 5–34. https://doi.org/10.1007/s11214-008-9336-1
Angelopoulos, V., Cruce, P., Schroeder, P., Grimes, E. W., Hatzigeorgiu, N., King, D. A., et al. (2019). The space physics environmental data analysis system (SPEDAS). *Space Science Reviews*, *215*(1), 9. https://doi.org/10.1007/s11214-018-0576-4
Balogh, A., Dunlop, M. W., Cowley, S. W. H., Southwood, D. J., Thomlinson, J. G., Glassmeier, K. H., et al. (1997). The Cluster Magnetic Field Investigation. *Space Science Reviews*, *79*(1/2), 65–91. https://doi.org/10.1023/a:1004970907748
Chaston, C. C., Bonnell, J. W., Carlson, C. W., McFadden, J. P., Strangeway, R. J., & Ergun, R. E. (2003). Kinetic effects in acceleration of auroral electrons in small scale Alfvén waves: A fast case study. *Geophysical Research Letters*, *30*(6), 1289. https://doi.org/10.1029/2002GL015777
Chaston, C. C., Bonnell, J. W., Peticolas, L. M., Carlson, C. W., & McFadden, J. P. (2002). Driven Alfvén waves and electron acceleration: A fast case study. *Geophysical Research Letters*, *29*(11), 1535. https://doi.org/10.1029/2001GL013842
Chaston, C. C., Peticolas, L. M., Bonnell, J. W., Carlson, C. W., Ergun, R. E., McFadden, J. P., & Strangeway, R. J. (2003). Width and brightness of auroral arcs driven by inertial Alfvén waves. *Journal of Geophysical Research*, *108*(2), 1091. https://doi.org/10.1029/2001JA007537
Claudepierre, S. G., Hudson, M. K., Lotko, W., Lyon, J. G., & Denton, R. E. (2010). Solar wind driving of magnetospheric ULF waves: Field line resonances driven by dynamic pressure fluctuations. *Journal of Geophysical Research*, *115*(A11), A11202. https://doi.org/10.1029/2010JA015399
Donovan, E., Mende, S., Jackel, B., Frey, H., Syrjasuo, M., Voronkov, I., et al. (2006). The THEMIS all-sky imaging array—System design and initial results from the prototype imager. *Journal of Atmospheric and Solar-Terrestrial Physics*, *68*(13), 1472–1487. https://doi.org/10.1016/j.jastp.2005.03.027
Elsden, T., & Wright, A. N. (2018). The broadband excitation of 3-D Alfvén resonances in a MHD waveguide. *Journal of Geophysical Research: Space Physics*, *123*(1), 530–547. https://doi.org/10.1002/2017JA025018
Fukuda, Y., Hirahara, M., Asamura, K., Sakanoi, T., Miyoshi, Y., Takada, T., et al. (2014). Electron properties in inverted-V structures and their vicinities based on Reimei observations. *Journal of Geophysical Research: Space Physics*, *119*(5), 3650–3663. https://doi.org/10.1002/2013JA018938
Glassmeier, K. H., & Stellmacher, M. (2000). Concerning the local time asymmetry of Pc5 wave power at the ground and field line resonance widths. *Journal of Geophysical Research*, *105*(A8), 18847–18855. https://doi.org/10.1029/2000JA900037
Goertz, C. K., & Boswell, R. W. (1979). Magnetosphere-ionosphere coupling. *Journal of Geophysical Research*, *84*(A12), 7239. https://doi.org/10.1029/JA084iA12p07239
Greenwald, R. A., & Walker, A. D. (1980). Energetics of long period resonant hydromagnetic waves. *Geophysical Research Letters*, *7*(10), 745–748. https://doi.org/10.1029/GL007i010p00745
Hasegawa, A. (1976). Particle acceleration by MHD surface waves and formation of the aurora. *Journal of Geophysical Research*, *81*(28), 5083–5090. https://doi.org/10.1029/JA081i028p05083
Hayashi, H., Koyama, Y., Hori, T., Tanaka, Y., Abe, S., Shinbori, A., et al. (2013). Inter-university upper atmosphere global observation network (IUGONET). *Data Science Journal*, *12*(0), WDS179–WDS184. https://doi.org/10.2481/dsj.WDS-030
Hudson, M. K., Lysak, R. L., & Mozer, F. S. (1978). Magnetic field aligned potential drops due to electrostatic ion cyclotron turbulence. *Geophysical Research Letters*, *5*(2), 143–146. https://doi.org/10.1029/GL005i002p00143
Humberset, B. K., Gjerloev, J. W., Samara, M., & Michell, R. G. (2017). Scale size-dependent characteristics of the nightside aurora. *Journal of Geophysical Research: Space Physics*, *122*(2), 2455–2466. https://doi.org/10.1002/2016JA023695
Ishisaka, K., Okada, T., Tsuruda, K., Hayakawa, H., Mukai, T., & Matsumoto, H. (2001). Relationship between the Geotail spacecraft potential and the magnetospheric electron number density including the distant tail regions. *Journal of Geophysical Research*, *106*(A4), 6309–6319. https://doi.org/10.1029/2000JA000077
Kageyama, A., Sugiyama, T., Watanabe, K., & Sato, T. (2006). A note on the dipole coordinates. *Computers & Geosciences*, *32*(2), 265–269. https://doi.org/10.1016/j.cageo.2005.06.006
Keiling, A., Wygant, J. W., Catell, C., Peria, W., Parks, G., Temerin, M., et al. (2002). Correlation of Alfvén wave Poynting flux in the plasma sheet at 4-7 Re with ionospheric energy flux. *Journal of Geophysical Research*, *107*(7), 1132–1145. https://doi.org/10.1029/2001JA900140

Kepko, L., Spence, H. E., & Singer, H. J. (2002). ULF waves in the solar wind as direct drivers of magnetospheric pulsations. *Geophysical Research Letters*, *29*(8), 1197–1201. https://doi.org/10.1029/2001GL014405

Kindel, J. M., & Kennel, C. F. (1971). Topside current instabilities. *Journal of Geophysical Research*, *76*(13), 3055–3078. https://doi.org/10.1029/JA076i013p03055

Lotko, W., Streltsov, V., & Carlson, C. W. (1998). Direct auroral arc, electrostatic shock and suprathermal electrons powered by dispersive, anomalously resistive field line resonance. *Geophysical Research Letters*, *25*(24), 4449–4452. https://doi.org/10.1029/1998GL900200

Mann, I. R., Wright, A. N., & Caully, P. S. (1995). Coupling of magnetospheric cavity modes to field line resonances: A study of resonance widths. *Journal of Geophysical Research*, *100*(A10), 19441–19450. https://doi.org/10.1029/95JA00820

Mende, S. B., Harris, S., Frey, H., Angelopoulos, V., Russell, C. T., Donovan, E., et al. (2008). The THEMIS array of ground- based observatories for the study of auroral substorms. *Space Science Reviews*, *141*, 357–387. https://doi.org/10.1007/978-0-387-89820-9_16

Newton, R. S., Southwood, D. J., & Hughes, J. F. (1978). Damping of geomagnetic pulsations by the ionosphere. *Planetary and Space Science*, *26*(3), 201–209. https://doi.org/10.1016/0032-0633(78)90085-5

Rankin, R., Gillies, D. M., & Degeling, A. W. (2021). On the relationship between shear Alfvén waves, auroral electron acceleration, and field line resonances. *Space Science Reviews*, *217*(4), 60. https://doi.org/10.1007/s11214-021-00830-x

Rankin, R., Kabin, K., Lu, J. Y., Mann, I. R., Marchand, R., Rae, I. J., et al. (2005). Magnetospheric field-line resonances: Ground-based observations and modeling. *Journal of Geophysical Research*, *110*(A10), A10S09. https://doi.org/10.1029/2004JA010919

Robinson, R. M., Vondrak, R. R., Miller, K., Dabbs, T., & Hardy, D. (1987). On calculating ionospheric conductances from the flux and energy of precipitating electrons. *Journal of Geophysical Research*, *92*(3), 2565–2569. https://doi.org/10.1029/JA092iA03p02565

Sakanoi, T., Fukunishi, H., & Mukai, T. (1995). Relationship between field-aligned currents and inverted-V parallel potential drops observed at midlatitudes. *Journal of Geophysical Research*, *100*(10), 19343–19360. https://doi.org/10.1029/95JA01285

Samson, J. C., Cogger, L. L., & Pao, Q. (1996). Observations of field line resonances, auroral arcs, and vortex structures. *Journal of Geophysical Research*, *101*(8), 17373–17383. https://doi.org/10.1029/96JA01086

Samson, J. G., Hughes, T. J., Creutzberg, F., Wallis, D. D., Greenwald, R. A., & Ruohoniemi, J. M. (1991). Observations of a detached discrete arc in association with field line resonances. *Journal of Geophysical Research*, *96*(A9), 15683–15695. https://doi.org/10.1029/91JA00796

Shepherd, S. G. (2014). Altitude-adjusted corrected geomagnetic coordinates: Definition and functional approximations. *Journal of Geophysical Research: Space Physics*, *119*(9), 7501–7521. https://doi.org/10.1002/2014JA020264

Shue, J.-H., Chao, J. K., Fu, H. C., Russell, C. T., Song, P., Khurana, K. K., & Singer, H. J. (1997). A new functional form to study the solar wind control of the magnetopause size and shape. *Journal of Geophysical Research*, *102*(A5), 9497–9511. https://doi.org/10.1029/97JA00196

Singer, H. J., Matheson, L., Grubb, R., Newman, A., & Bouwer, S. D. (1996). Monitoring space weather with the GOES magnetometers. *Proceedings of the Society of Photo-Optical Instrumentation Engineers*, *2812*, 299–308. https://doi.org/10.1117/12.254077

Singer, H. J., Southwood, D. J., Walker, R. T., & Kivelson, M. G. (1981). Alfven wave resonances in a realistic magnetospheric magnetic field geometry. *Journal of Geophysical Research*, *86*(A6), 4589–4596. https://doi.org/10.1029/JA086iA06p04589

Takahashi, K., & Denton, R. E. (2021). Nodal structure of toroidal standing Alfvén waves and its implication for field line mass density distribution. *Journal of Geophysical Research: Space Physics*, *126*(5), e2020JA028981. https://doi.org/10.1029/2020JA028981

Takahashi, K., Vellante, M., Corpo, A. D., Claudepierre, S. G., Kletzing, C., Wygant, J., & Koga, K. (2019). Multiharmonic toroidal standing Alfvén waves in the midnight sector observed during a geomagnetically quiet period. *Journal of Geophysical Research: Space Physics*, *124*(3), e2019JA027370. https://doi.org/10.1029/2019JA027370

Tsyganenko, N. A., & Sitnov, M. I. (2005). Modeling the dynamics of the inner magnetosphere during strong geomagnetic storms. *Journal of Geophysical Research: Space Physics*, *110*(A3), A03208. https://doi.org/10.1029/2004JA010798

Vaivads, A., Andre, M., Buchert, S., Eriksson, A. I., Olson, A., Wahluad, J. E., et al. (2003). What high altitude observations tell us about the auroral acceleration: A cluster/DMSP conjunction. *Geophysical Research Letters*, *30*(3), 1106. https://doi.org/10.1029/2002GL016006

Wang, B., Nishimura, Y., Zhang, H., Shen, X. C., Lyons, L., Angelopoulos, V., et al. (2019). The 2- D structure of foreshock- driven field line resonances observed by THEMIS satellite and ground- based imager conjunctions. *Journal of Geophysical Research: Space Physics*, *124*(8), 6792–6811. https://doi.org/10.1029/2019JA026668

Wright, A. N. (1992). Asymptotic and time-dependent solutions of magnetic pulsations in realistic magnetic field geometries. *Journal of Geophysical Research*, *97*(A5), 6439–6450. https://doi.org/10.1029/91JA02666

Wright, A. N., & Allan, W. (1996). Structure, phase motion, and heating within Alfven resonances. *Journal of Geophysical Research*, *101*(A8), 17399–17408. https://doi.org/10.1029/96JA01141

Wright, A. N., Allan, W., & Damiano, P. A. (2003). Alfvén wave dissipation via electron energization. *Geophysical Research Letters*, *30*(16), 1847. https://doi.org/10.1029/2003GL017605

Wright, A. N., Allan, W., Elphinstone, R. D., & Cogger, L. L. (1999). Phase mixing and phase motion of Alfvén waves on tail-like and dipole-like magnetic field lines. *Journal of Geophysical Research*, *104*(A5), 10159–10176. https://doi.org/10.1029/1999JA900018

Wright, A. N., Allan, W., Ruderman, M. S., & Elphic, R. C. (2002). The dynamics of current carriers in standing Alfvén waves. Parallel electric fields in auroral acceleration region. *Journal of Geophysical Research*, *107*(A7), 1120. https://doi.org/10.1029/2001JA900168

Wright, A. N., & Elsden, T. (2020). Simulations of MHD wave propagation and coupling in a 3-D magnetosphere. *Journal of Geophysical Research: Space Physics*, *125*(2), e2019JA027589. https://doi.org/10.1029/2019JA027589

Wright, A. N., & Hood, A. W. (2003). Field-aligned electron acceleration in Alfvén waves. *Journal of Geophysical Research*, *108*(A3), 1135. https://doi.org/10.1029/2002JA009551

Wygant, J. R., Keiling, A., Cattell, C. A., Johnson, M., Lysak, R. I., Tenerin, M., et al. (2000). Polar spacecraft based comparisons of intense electric fields and poynting flux near and within the plasma sheet-tail lobe boundary to UVI images: An energy source for the aurora. *Journal of Geophysical Research*, *105*(A8), 18675–18692. https://doi.org/10.1029/1999JA900500

Wygant, J. R., Keiling, A., Cattell, C. A., Lysak, R. L., Temerin, M., Mozer, F. S., et al. (2002). Evidence for kinetic Alfvén waves and parallel electron energization at 4–6 RE altitudes in the plasma sheet boundary layer. *Journal of Geophysical Research*, *107*(A8), 1201. https://doi.org/10.1029/2001JA900113

Xu, B.-I., Samson, J. C. S., Liu, W. W., Creutzber, F., & Hughes, T. J. (1993). Observations of optical aurora modulated by resonant Alfvén waves. *Journal of Geophysical Research*, *98*(A7), 11531–11541. https://doi.org/10.1029/93JA00435

Zhao, H. Y., Zhou, X. Z., Ying, L., Gang, R. R., Wang, Y., Shi, Q. Q., et al. (2019). Poleward-moving recurrent auroral arcs associated with impulse-excited standing hydromagnetic waves. *Earth and Planetary Physics*, *3*(4), 305–313. https://doi.org/10.26464/epp2019032